Peer-reviewed version available at *Cancers* **2020**, *12*, 2647; doi:10.3390/cancers12092647

Article

Inhibition of DNA repair pathways and induction of ROS are potential mechanisms of action of the small molecule inhibitor BOLD-100 in breast cancer

Suzanne Bakewell[1], Isabel Conde[2], Yassi Fallah[2], Mathew McCoy[2,3], Lu Jin[2] and Ayesha N. Shajahan-Haq[2],*

[1] Intezyne Technologies, Tampa, FL; bakewellsj@gmail.com (S.B.)
[2] Georgetown University Medical Center, Department of Oncology, Lombardi Comprehensive Cancer Center, Washington, DC; [3]Innovation Center for Biomedical Informatics (ICBI), Georgetown University Medical Center, Washington, DC; isabelconde@gmail.com (I.C.); yf120@georgetown.edu (Y.F.); lj74@georgetown.edu (L.J.); mdm299@georgetown.edu (M.M.); ans33@georgetown.edu (A.N.S-H.)
* Correspondence: ans33@georgetown.edu

Abstract: BOLD-100, a ruthenium-based complex, sodium trans-[tetrachloridobis(1H-indazole)ruthenate(III)] (also known as IT-139, NKP1339 or KP1339), is a novel small molecule drug that demonstrated a manageable safety profile at the maximum tolerated dose and modest antitumor activity in a phase I clinical trial. BOLD-100 has been reported to inhibit the upregulation of the endoplasmic reticulum stress sensing protein GRP78. However, response to BOLD-100 varies in different cancer models and the precise mechanism of action in high-response versus low-response cancer cells remains unclear. *In vitro* studies have indicated that BOLD-100 induces cytostatic rather than cytotoxic effects as a monotherapy. To understand BOLD-100 mediated signaling mechanism in breast cancer cells, we used estrogen receptor positive (ER+) MCF7 breast cancer cells to obtain gene-metabolite integrated models. Particularly, BOLD-100 significantly reduced expression of genes involved in the DNA repair pathway. BOLD-100 also induced reactive oxygen species (ROS) and phosphorylation of histone H2AX, ⊚H2AX (Ser139), suggesting disruption of proper DNA surveillance. In estrogen receptor negative (ER-) breast cancer cells, combination of BOLD-100 with a PARP inhibitor, olaparib, induced significant inhibition of cell growth and xenografts and increased ⊚H2AX. Thus, BOLD-100 is a novel DNA repair pathway targeting agent and can be used with other chemotherapies in ER- breast cancer.

Keywords: breast cancer; BOLD-100; olaparib; triple negative breast cancer

1. Introduction

In the United States, about 150,000 patients are currently living with metastatic breast cancer. While targeted therapies have improved survival, metastatic breast cancer remains an incurable disease. Therefore, there is an urgent need for developing therapies that could provide novel treatment options for such patients. Breast cancer is a heterogeneous disease that is broadly classified into hormone-receptor-positive, estrogen receptor positive [ER+] and progesterone receptor positive [PR+] (ER+/PR+), human epidermal growth factor receptor-2 overexpressing (HER2+) or triple-negative breast cancer (TNBC; lacks ER, PR and HER2). 70% of all breast cancers are ER+/PR+ and are treated with endocrine therapy that block ER activity with antiestrogens such as Tamoxifen or Faslodex/Fulvustrant/ICI or aromatase inhibitors such as letrozole [1,2]. Advanced ER+/PR+ disease is currently treated with endocrine therapy and CDK4/6 inhibitors [3-5]. HER2 is overexpressed in 15-20% of breast cancers and treatment is targeted with anti-HER2 targeting agents [6]. TNBC constitutes about 10-15% of all breast cancers [7], and although BRCA-associated TNBC is treated with PARP inhibitors (e.g., olaparib), this subtype remains without a defined drug target and is treated with chemotherapies [8]. In addition to these histological classifications, other factors such as

Peer-reviewed version available at Cancers 2020, 12, 2647; doi:10.3390/cancers12092647

menopausal status, lymph node invasion and tumor size are considered to determine the best therapeutic option. However, the ability of cancer cells to evade cell death and to develop drug resistance remains a major clinical hurdle [9-11]. Therefore, novel therapies that are effective in inducing cell death in combination with standard of care therapies are urgently needed to improve survival in breast cancer patients.

BOLD-100 is an intravenously administered small molecule shown to be well tolerated with modest anti-tumor activity in a Phase I clinical trial [12]. A high affinity for albumin and unique chemistry allow increased activation of BOLD-100 within tumors cells. BOLD-100's mechanism has recently shown to be partly due to the suppression of GRP78 at the mRNA and protein level in stressed or drug resistant cancer cells in a context-dependent manner [13-15]. In this study, we treated non-stressed breast cancer cells with BOLD-100 and established an integrated signaling network to look at significantly altered genes and metabolites. This integrated signaling network showed that BOLD-100 altered DNA repair pathways. Both *in vitro* and *in vivo* studies show that BOLD-100 is a useful combination strategy with other DNA targeting drugs, particularly, the PARP-inhibitor olaparib in TNBC. Thus, BOLD-100 may be beneficial in combination with other treatment strategies that target DNA repair pathways in cancer.

2. Results

2.1. BOLD-100 inhibits growth of breast cancer cells

To determine the effect of BOLD-100 in non-stressed breast cancer cells, we treated both ER+ [MCF7, MCF7(2), MDA-MB-175] and TNBC [MDA-MB-231, MDA-MB468] breast cancer cells in regular cell culture media under basal conditions with BOLD-100 ranging from 10 to 200 ◎M for 72 h (Figure 1A-E). Since cell growth rates vary in the different cell lines, we used t=0 to compare the net growth at 72 h with vehicle (DMSO) alone or different doses of BOLD-100. All cells showed varying levels of sensitivity to BOLD-100 at different doses. For all cells, growth was significantly ($p<0.05$) inhibited for all cell lines with 100 ◎M BOLD-100 compared with vehicle at 72 h. Particularly, MCF7(2), MDA-MB-231 and MDA-MB-468 cells showed increased sensitivity to BOLD-100 in a dose-dependent manner. Time-course studies with 0, 10 or 100 ◎M BOLD-100 showed significant ($p<0.04$) decrease in cell proliferation with 100 ◎M compared with 0 ◎M BOLD-100 at 72 h in MCF7(2), MDA-MB-175, MDA-MB-231 and MDA-MB-468 cells (Figure 1F-I). Analysis of cell cycle in MCF7(2) and MDA-MB-231 cells, two cell lines that showed increased sensitivity ($p<0.05$), showed significant increase in cells in G2/M phase treated with 100 ◎M BOLD-100 compared with vehicle (Figure 2A and B). Therefore, BOLD-100 mediated inhibition of cell proliferation involves G2/M cell cycle arrest.

2.2. Significantly altered genes, metabolites and proteins in BOLD-100 treated cells show changes in DNA repair pathways

Previously, it has been shown that BOLD-100 inhibits upregulation of GRP78 in stressed cancer cells [13]. To determine the molecular changes associated with BOLD-100 treatment in non-stressed cells, we analyzed and integrated the signaling pathways associated with significantly changed genes and metabolites in MCF7(2) cells (Figure 3A). We selected MCF7(2) cells for molecular analysis based on their high sensitivity to BOLD-100 as demonstrated by cell growth studies shown above (Figure 1). MCF7(2) cells were treated with vehicle alone or 100 ◎M BOLD-100 for 72 h followed by transcriptomics and metabolomics analysis (see Methods for details). Network analysis of the top 2000 differentially expressed genes, ranked by p-value, [IPA Core Analysis (QIAGEN Inc., Redwood City, CA)] identified disease and functional pathways enriched in differentially expressed genes (Supplemental Table S1). Networks of differentially expressed genes were input into STITCH [20] along with differentially expressed metabolites, to integrate the gene expression datasets and expand the networks to include common interacting neighbors from the STITCH database. The resulting networks for each differentially expressed set were integrated and pruned of both nodes not detected as differentially expressed in the dataset including subnetworks isolated from the largest interconnected sets. The networks were visualized using Cytoscape [21] with genes represented as

Peer-reviewed version available at Cancers 2020, 12, 2647; doi:10.3390/cancers12092647

rectangles and metabolites as triangles, with the log2-fold change overlaid scaled from low (green) to high (red) expression (Figure 3A). Gene expression levels for GRP78 was not changed in treated versus control cells in this analysis, which was further validated by assessing GRP78 protein levels with western blot analysis (Supplementary Figure S1 A). Differentially expressed genes-metabolites network comprised several genes associated with DNA damage response that were significantly decreased, such as ATM, CHEK1, BRCA1, CDC25A while cell cycle arrest genes were significantly increased, such as CDKN1A(p21) and LIN9 (Figure 3A). Selected proteins coded by the genes in the network was validated by western blot analysis in MCF7(2) cells treated with 0, 10 or 100 ◎M Bold-100 for 72 h to show the dose-dependent effect of the drug on protein levels (Figure 3B and C). We Interestingly, CYP1B1, a metabolizing enzyme involved in processing of xenobiotics or drugs [24] was increased at both the gene and protein levels (Figure 3A and C). Furthermore, mass spectrometry based quantitative measurement of citric acid and isocitrate, critical intermediates of the Tricarboxylic Acid Cycle (TCA cycle), showed 11-fold elevated in BOLD-100 treated cells compared to control (Figure 3D). Furthermore, high throughput analysis of proteins using Reverse Phase Protein Array (RPPA) in MCF7(2) cells treated with vehicle or 100 ◎M BOLD-100 for 72 h showed significant decrease in cell cycle proteins such as RAD51, PCNA, ATM and ATRX (Table 1), consistent with the gene expression analysis.

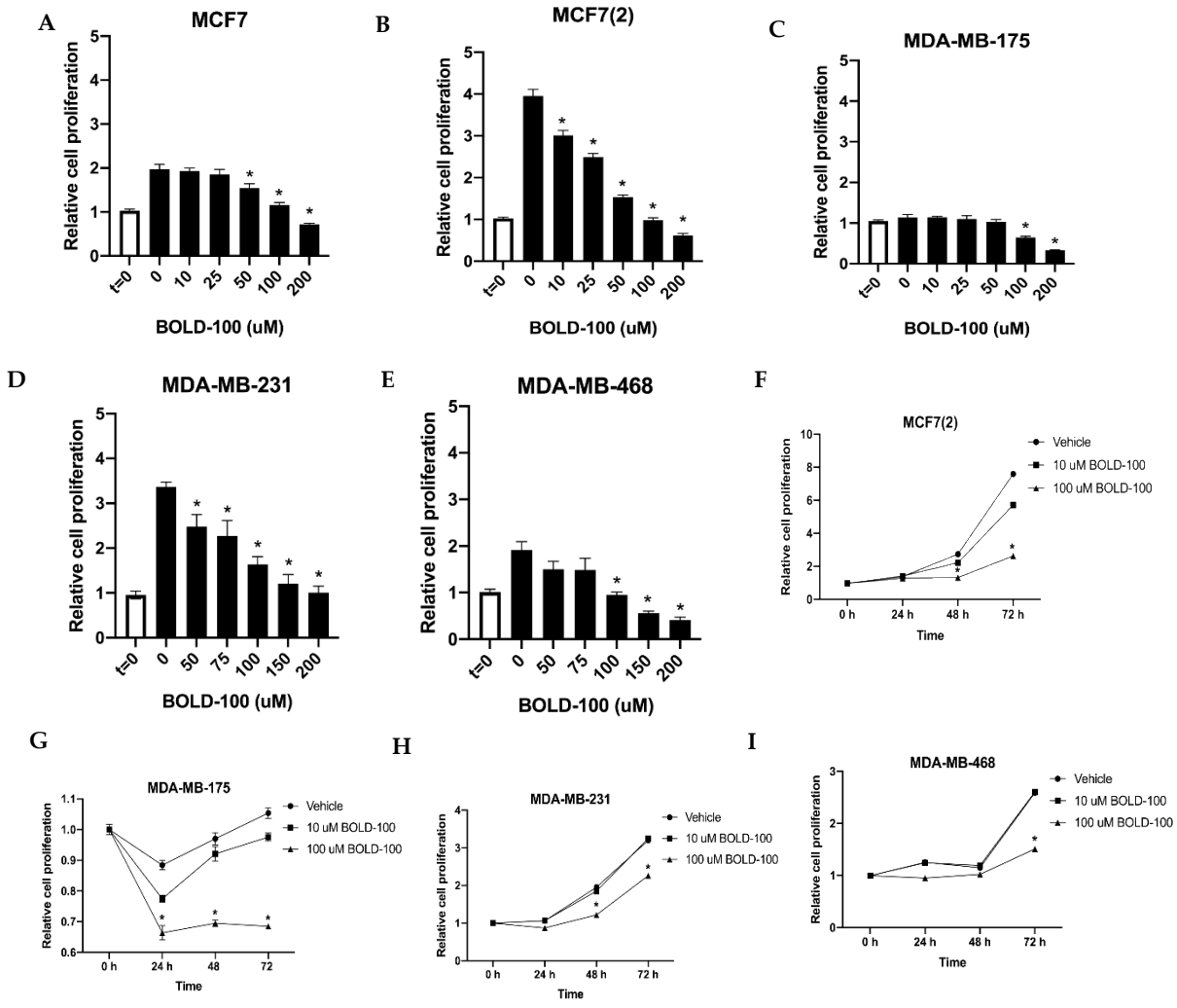

Figure 1. BOLD-100 inhibited growth of breast cancer cells. Estrogen receptor positive (ER+) breast cancer cells [MCF7, MCF7(2) and MDA-MB-175] and estrogen receptor negative (ER-) breast cancer cells (MDA-MB-231 and MDA-MB-468) were treated with indicated concentrations of BOLD-100 for 72 h and compared to time=0 (at the onset of treatment). (A) MCF7(2), (B) MCF7, (C) MDA-MB-175, (D) MDA-MB-231 and (E) MDA-MB-468 cells were significanlty (*p<0.05) inhibited by 100 μM BOLD-

Peer-reviewed version available at Cancers 2020, 12, 2647; doi:10.3390/cancers12092647

100. Time-course (24, 48 and 72 h) with 0, 10 or 100 µM BOLD-100 showed significant (*p<0.04) inhibition of (F) MCF7(2), (G) MDA-MB-175, (H) MDA-MB-231 and (I) MDA-MB-468 cells with 100 µM compared with 0µM BOLD-100 at 72 h. ANOVA, $p < 0.01$; *$p < 0.05$ for conditions in indicated cells compared with control.

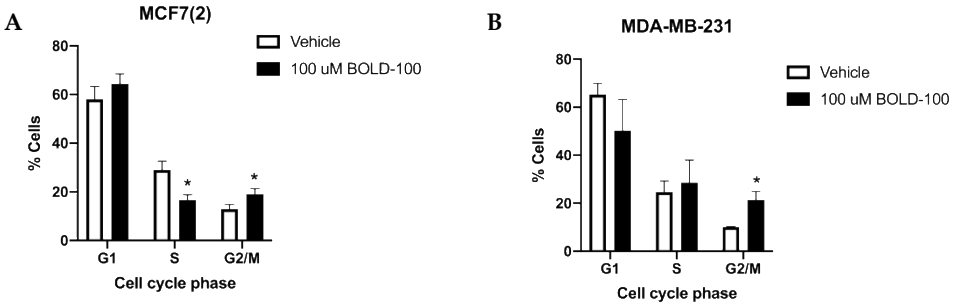

Figure 2. BOLD-100 treatment arrested breast cancer cells in G2/M phase of the cell cycle. Cell cycle analysis of (A) MCF7(2) and (B) MDA-MB-231 cells with 100 µM of BOLD-100 showed significant decrease in S phase and increase in G2/M compared with vehicle treated cells. ANOVA, $p < 0.01$; *$p < 0.05$ for respective cell cycle phase in cells treated with 100 µM BOLD-100 compared with cells treated with vehicle.

2.3. BOLD-100 induces reactive oxygen species (ROS)

Since DNA repair pathway genes were significantly increased in BOLD-100 treated cells, we compared total cellular ROS in untreated and treated cells. ROS can induce DNA damage and trigger a complex signaling mechanism called the DNA damage response (DDR) that is used by the cell to reset genomic stability [25]. In MCF7(2), MDA-MB-231 and MDA-MB-468 cells, treatment with BOLD-100 increased ROS levels in a dose-dependent manner (Figure 4A-C) compared with vehicle treated cells (negative control). In fact, at 100 and 200 ◎M, BOLD-100 induced more ROS than 100 ◎M tert-butyl hydroperoxide (TBHP), which is a positive control for inducing cellular ROS [26]. Thus, these data suggest that the anti-proliferative effects of BOLD-100 in breast cancer cells is partly due to ROS-dependent cellular damage.

2.4. BOLD-100 synergizes with anticancer agents that target DNA in TNBC cells

Drugs that target DNA synthesis or repair pathways are often used to treat TNBC. For example, olaparib, an inhibitor of the enzyme poly ADP ribose polymerase (PARP); capecitabine, an oral antimetabolite that interferes with DNA synthesis; or carboplatin, a DNA damaging agent [27]. Hence, we tested the efficacy of BOLD-100 in combination with these DNA targeting agents in TNBC cells. MDA-MB-231 and MDA-MB-468 cells were treated with increasing doses of olaparib, capecitabine or carboplative in combination with 100 ◎M BOLD-100. For all conditions, t=0 was included to compare growth rates of cells under different conditions from the onset of treatments. Synergestic interactions were analyzed by calculating RI values (see Materials and Methods; RI >1 indicates synergy). In MDA-MB-231 cells, combination of BOLD-100 and olaparib synergistically inhibited cell proliferation at all concentrations from 1◎◎M (R=1.21), 5 ◎M (R=1.06), 10◎◎M (R=1.04) and 20 ◎M (R=1.25) olaparib compared with BOLD-100 alone. In MDA-MB-468 cells, combination of BOLD-100 and olaparib synergistically inhibited cell proliferation at 10 ◎M (RI=1.26) and 20 ◎M (R=1.14) (Figure 5A-B). For capecitabine, 100 ◎M BOLD-100 synergized with 100 ◎M (R=1.91) and 200 ◎M (R=1.92) of the drug (Figure 5 C-D) in both MDA-MB-231 and MDA-MB-468 cells. For carboplatin, BOLD-100 synergized with 50 ◎M (R=1.75), 75◎◎M (R=1.34) and 100 ◎M (R=1.26) carboplatin in MDA-MB-231 cells but only with 75◎M carboplatin in MDA-MB-468 cells (Figure 5E-F).

Peer-reviewed version available at Cancers 2020, 12, 2647; doi:10.3390/cancers12092647

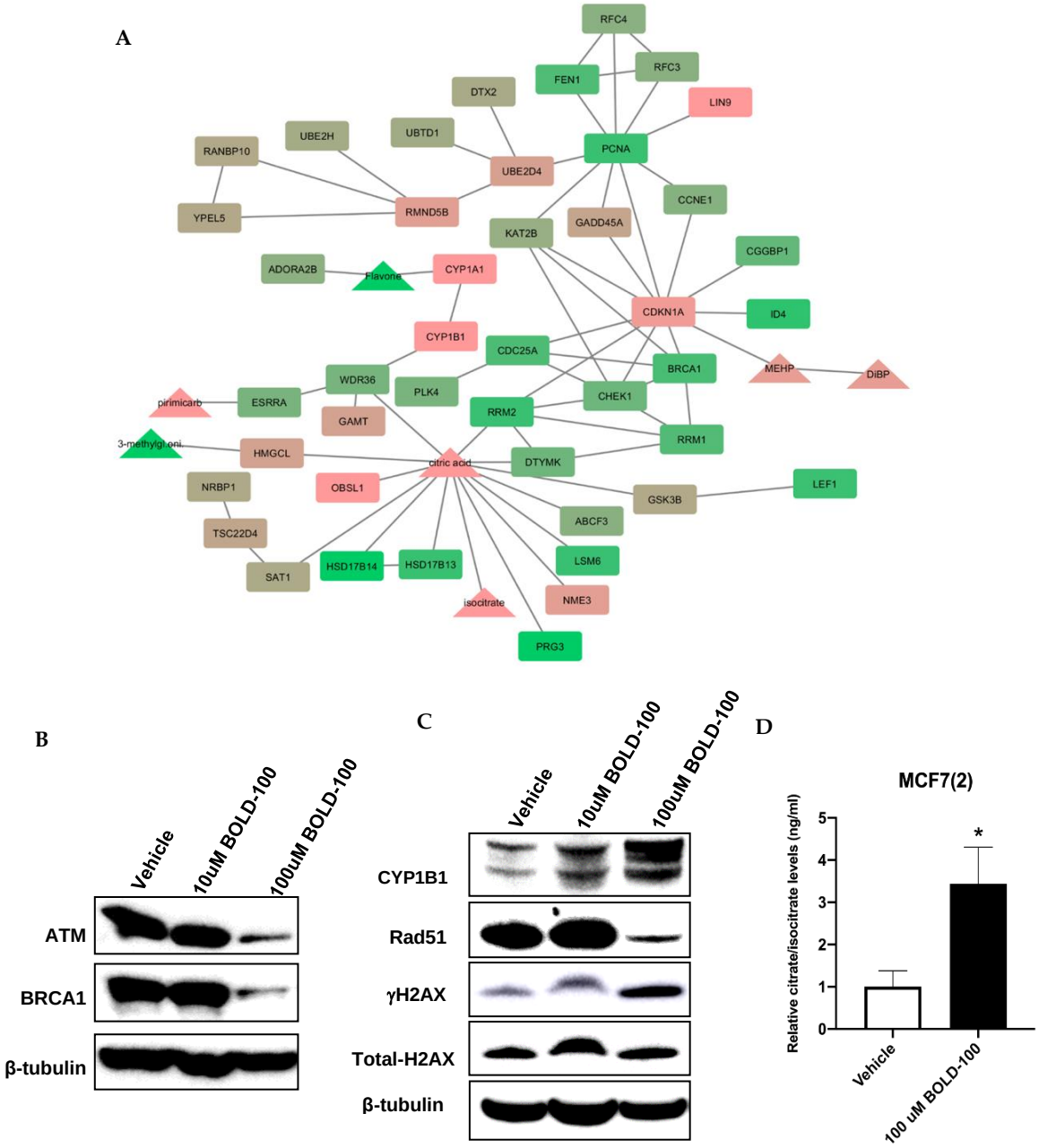

Figure 3. Integration of significantly altered genes and metabolites in MCF7(2) cells treated with 100 μM BOLD-100 for 72 h. (A) Network analysis of the top 2000 differentially expressed (DE) genes, ranked by p-value. Each of the mutually exclusive networks of DE genes were input into STITCH along with all DE metabolites to integrate the gene and protein expression datasets and expand the networks to include common interacting neighbors from the STITCH database. The resulting networks for each DE set were integrated and pruned of both nodes not detected as differentially expressed in the dataset including subnetworks isolated from the largest interconnected sets. The networks were visualized using Cytoscape, with genes represented as rectangles and metabolites as triangles, with the log2 fold change overlaid scaled from low (green) to high (red) expression. B-D, Validation of gene-metabolite integration model in MCF7(2) cells. Western blot analysis in cells treated with vehicle (DMSO), 10 μM or 100 μM BOLD-100 for 72 h show (A) ATM and BRCA1 protein levels were decreased with 100 μM BOLD-100 treatment, (B) CYP1B1 and γH2AX (marker of DNA double-strand break) was increased (total H2AX levels did not change) while RAD51 protein level was decreased with 100 μM BOLD-100 treatment.

Peer-reviewed version available at Cancers 2020, 12, 2647; doi:10.3390/cancers12092647

Table 1. Reserve phase protein array (RPPA) results with significantly altered proteins in MCF7 cells treated with 100 μM BOLD-100 compared with control.

PROTEIN NAME	p-value	% Difference in 100 μM BOLD-100 treated cells
Rab11	<0.001	19% increased
PDK1	<0.001	24% increased
Notch3	<0.001	16% increased
TSC1	<0.001	27% increased
14-3-3-beta	<0.001	12% increased
p38-MAPK	<0.001	16% increased
SOD2	<0.001	22% increased
G6PD	<0.001	39% increased
NAPSIN	<0.001	11% decreased
PI3K-p85	0.001	6% increased
HER2	0.002	31% increased
ACC1	0.002	13% increased
PEA-15	0.002	12% increased
PCNA	0.002	8% decreased
Raptor	0.002	5% decreased
RSK	0.002	11% increased
DM-K9-Histone-H3	0.003	6% decreased
Rad51	0.003	10% decreased
HSP70	0.004	18% increased
PDK1_pS241	0.004	35% increased
Rock-1	0.004	18% increased
CD44	0.004	7% decreased
Jak2	0.004	15% decreased
ATM	0.005	18% decreased
Oct-4	0.005	6% decreased
b-Catenin	0.005	7% decreased
P-Cadherin	0.005	12% increased
Transglutaminase	0.005	5% increased
D-a-Tubulin	0.005	8% increased
Notch1	0.006	21% increased
TFAM	0.006	30% increased
INPP4b	0.007	19% increased
Chk2	0.007	8% decreased
Chk1_pS296	0.007	4% decreased
14-3-3-zeta	0.009	17% increased
PR (Progesterone receptor)	0.009	64% decreased
DJ1	0.010	24% increased
⌾-Actin	0.010	13% increased
Annexin-VII	0.010	16% increased
p27_pT198	0.011	14% decreased
MAPK_pT202_Y204	0.013	7% decreased
p70-S6K1	0.013	15% increased
ATR_pS428	0.014	12% decreased
TIGAR	0.014	15% increased
MUC1 (EMA)	0.014	65% increased
UGT1A	0.015	36% increased
RBM15	0.015	19% decreased
FRA-1	0.016	7% increased
TUFM	0.017	16% decreased
Bax	0.017	12% increased
Smad4	0.019	4% decreased
HER2_pY1248	0.020	6% increased
MEK1	0.020	7% increased

Peer-reviewed version available at Cancers 2020, 12, 2647; doi:10.3390/cancers12092647

Stat3	0.021	9% increased
PKCa	0.021	4% increased
MSI2	0.022	10% decreased
RPA32	0.022	5% decreased
p53	0.022	7% increased
AMPK-a2_pS345	0.023	12% decreased
Collagen-VI	0.025	21% increased
c-Jun_pS73	0.026	20% decreased
Smad3	0.026	8% decreased
ATM_pS1981	0.027	3% decreased
TAZ	0.030	13% increased
HER3	0.031	9% increased
ATRX	0.031	24% decreased
Cyclin-E1	0.031	18% increased
Mcl-1	0.031	15% increased
TWIST	0.032	6% decreased
Elk1_pS383	0.032	4% decreased
LC3A-B	0.035	21% increased
IR-b (INSRB)	0.038	9% increased
Rb	0.038	4% decreased
PKC-b-II_pS660	0.039	10% increased
WIPI2	0.042	4% decreased
Ets-1	0.042	7% decreased
Stathmin-1	0.042	3% decreased
Paxillin	0.043	11% increased
IRS1	0.043	16% decreased
Cyclin-D3	0.044	39% increased
ERCC5	0.045	5% increased
p27-Kip-1	0.048	2% decreased

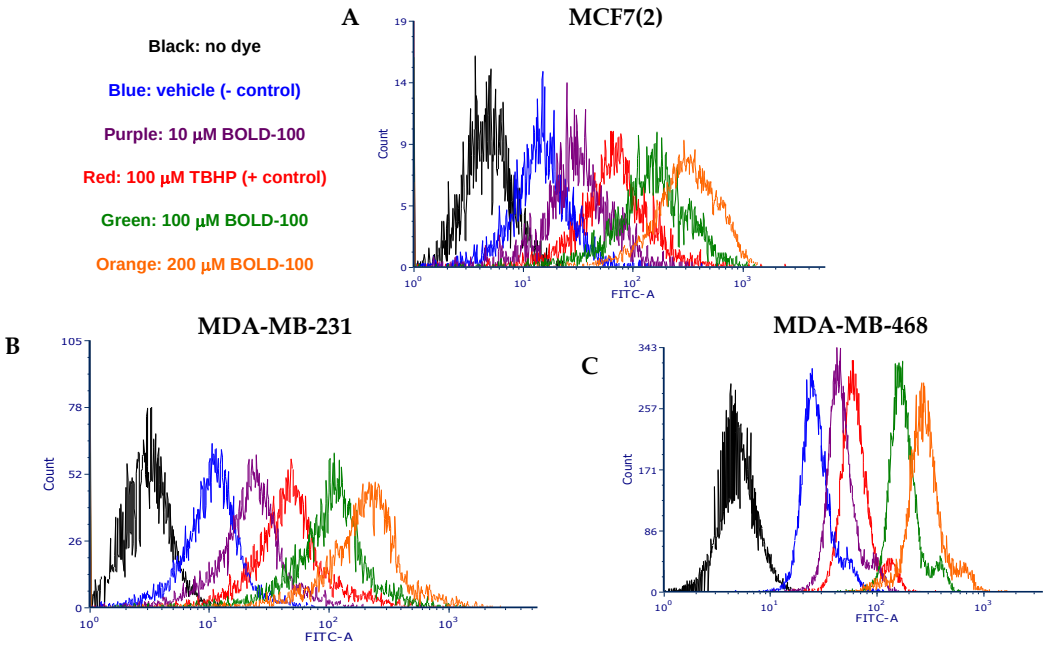

Figure 4. BOLD-100 induced ROS and increased autophagosomes levels in TNBC cells. Cell permeant reagent 2′,7′ –dichlorofluorescin diacetate (DCFDA) was used to measure cellular ROS activity (FITC-A, x-axis) in within cells (count, y-axis). BOLD-100 induced ROS increased in a dose-dependent manner in (A) MCF(2), (B) MDA-MB-231 and (C) MDA-MB-468 cells. Negative control was vehicle (DMSO alone) and positive control was 100 µM Tert-Butyl Hydrogen Peroxide (TBHP) for 6 h.

Peer-reviewed version available at Cancers 2020, 12, 2647; doi:10.3390/cancers12092647

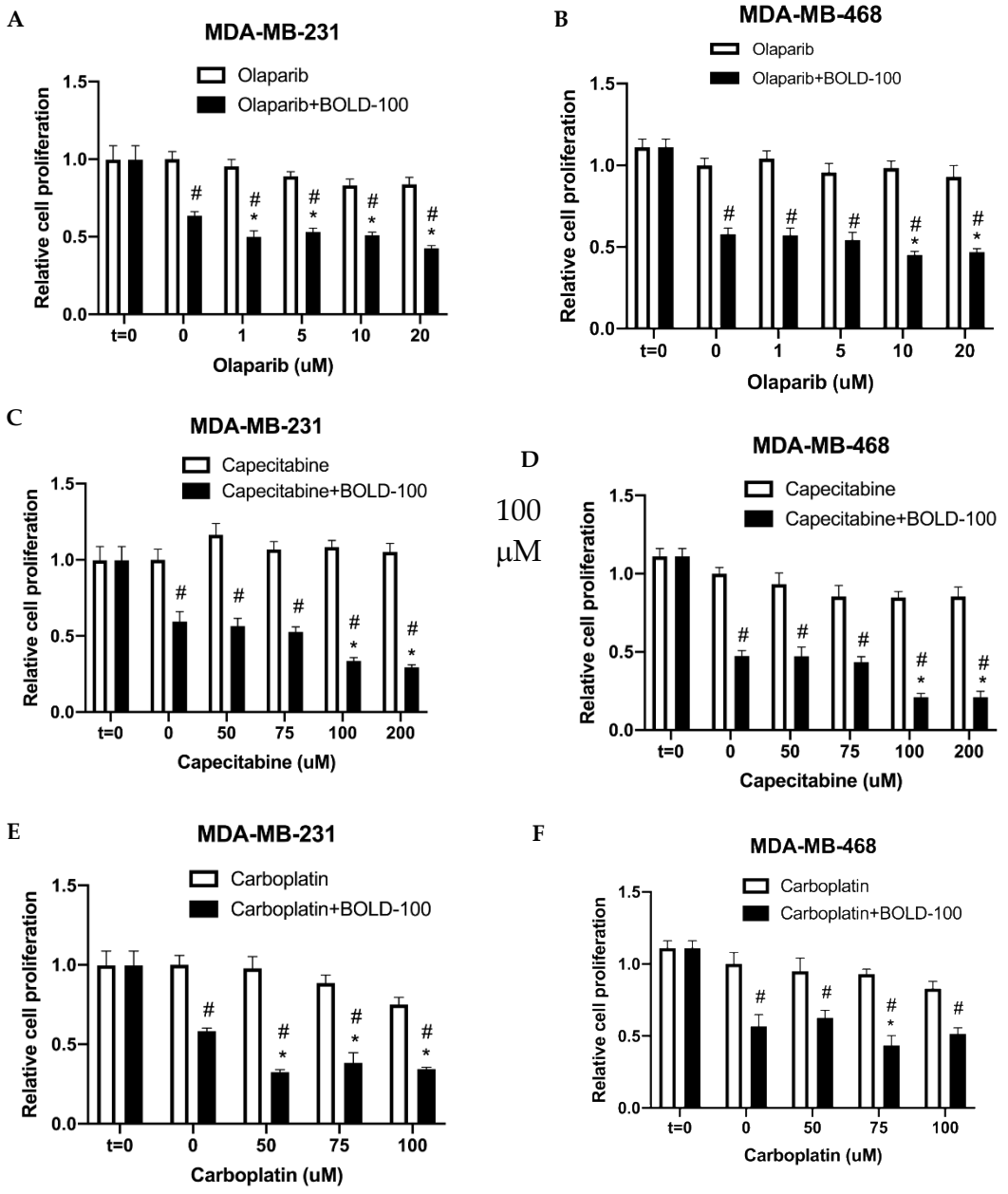

Figure 5. BOLD-100 suppressed growth of TNBC breast cancer cells and tumors in combination with anticancer drugs that target the DNA. Cell proliferation was measured using a crystal violet method. Synergestic interactions were analyzed by calculating RI values (see Materials and Methods; RI >1 indicates synergy). (A) MDA-MB-231 and (B) MDA-MB-468 cells were treated with varying concentrations of olaparib and 100 μM BOLD-100. (C) MDA-MB-231 and (D) MDA-MB-468 cells were treated with varying concentrations of capecitabine and 100 μM BOLD-100. (E) MDA-MB-231 and (F) MDA-MB-468 cells were treated with varying concentrations of caboplatin and 100 μM BOLD-100. ANOVA, $p < 0.001$; #$p < 0.05$ for treatment versus control for respective cell lines; *$p < 0.05$ for treatment versus 0 μM for specific drug in respective cell lines.

To further elucidate how BOLD-100 increases efficacy of DNA targeting anticancer drugs, we focused on the combination of olaparib and BOLD-100. In cancer cells, ROS has been implicated in mediating therapeutic response [28] by inducing DNA damage. Particularly, double stranded breaks (DSB) in DNA is commonly detected with phosphorylation (S139) of the histone H2AX (γH2AX) [29,30]. Since we showed that BOLD-100 induces ROS (Figure 4), to assess whether BOLD-100

Peer-reviewed version available at Cancers 2020, 12, 2647; doi:10.3390/cancers12092647

induced DSB, we analyzed ◎H2AX protein in TNBC cells treated with BOLD-100 and/or olaparib (Figure 6A). When treated with both olaparib (10 ◎M) and BOLD-100 (100 ◎M), increased levels of ◎H2AX were observed in both MDA-MB-231 and MDA-MB-468 cells relative to treatments with individual drugs or vehicle alone. While treatment with BOLD-100 or olaparib alone did not increase ◎H2AX protein levels in MDA-MB-231 cells, these drugs increased ◎H2AX levels in MDA-MB-468 cells as single agents compared with vehicle. However, in both cells, ◎H2AX levels were most pronounced with combination of both drugs.

To better understand the mode of cell death pathway following this combination treatment, we evaluated levels of autophagy and apoptosis (Figure 6B-D). MDA-MB-231 cells treated with Bold-100 alone or in combination with olaparib increased accumulation of autophagosome marker, LC3IIB, and autophagosome cargo protein, p62 (SQSTM1) (Figure 6B). Both LC3IIB and p62 were increased, which implies a blockage of autophagy [31]. Measurement of autophagosomes using CytoID dye that accumulates within autophagosomes showed significantly ($p<0.001$) increased levels of these vacuoles in cells treated with olaparib and Bold-100 compared with vehicle alone (Figure 6C). Cells that were serum started for 24 h was used as positive control. Furthermore, measurement of apoptotic cells using annexin-V (see Materials and Methods) in MDA-MB-231 cells showed significantly more cells undergoing apoptosis when treated with olaparib and Bold-100 compared to vehicle treated cells. Doxorubicin (10nM) was used as a positive control to induce apoptosis. Together, these data suggest that combination of olaparib and BOLD-100 blocked autophagic flux and induced cell death via apoptosis.

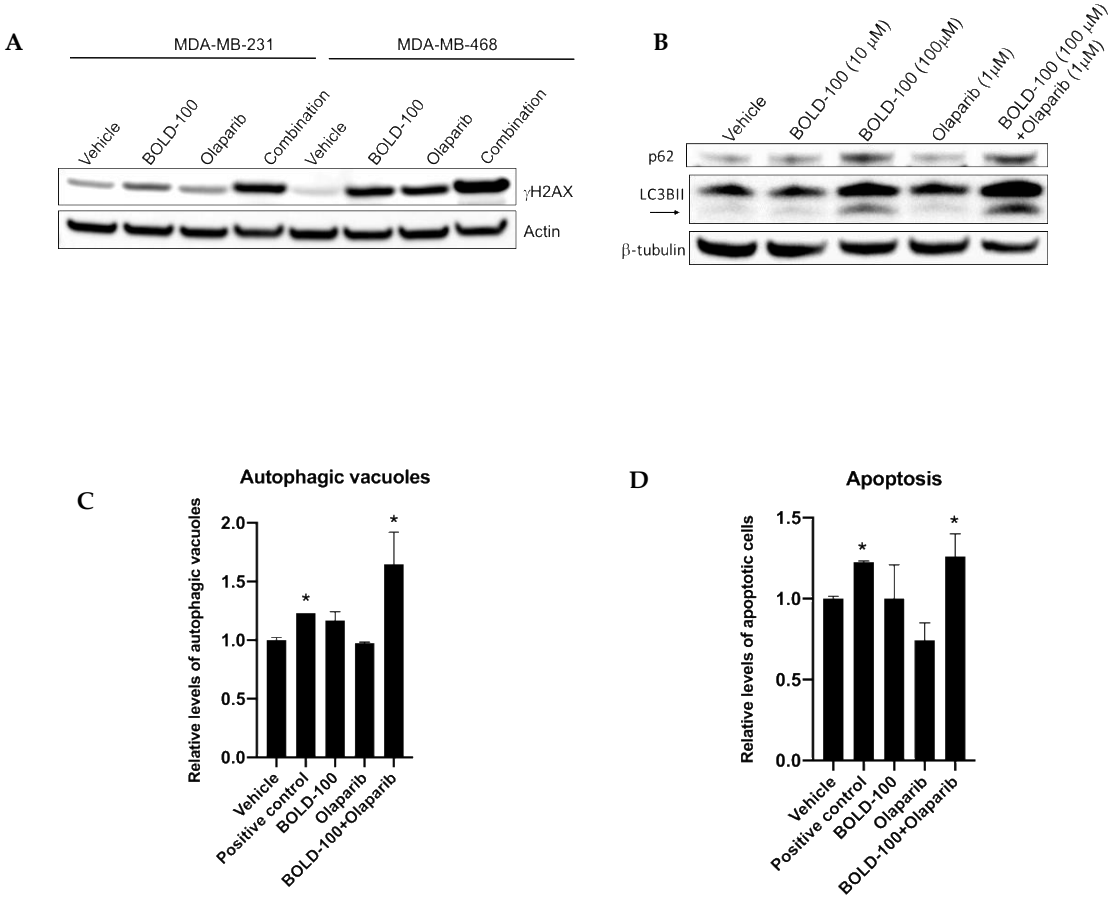

Figure 6: Combination of BOLD-100 and olaparib induces ⚜H2AX and cell death in TNBC cells. (A) Increased ◎H2AX protein levels were detected by Western blotting in MDA-MB-231 and MDA-MB-468 cells following treatment with both BOLD-100 and olaparib compared with vehicle control

Peer-reviewed version available at Cancers 2020, 12, 2647; doi:10.3390/cancers12092647

for 72 h. Actin was used as a loading control. (B) Western blot analysis in MDA-MB-231 cells treated with BOLD-100 (100 ⊙M) or BOLD-100 (100 ⊙M)+olaparib (1 ⊙M) showed increased LC3II (autophagosome marker) and p62 (marker of autophagy activity). ⊙-tubulin was used as a loading control. (C) Cyto-ID assay (Enzo, Farmingdale, NY) was used to measure autophagic vacuoles in MDA-MB-231 cells using flow cytometry: vehicle alone, positive control (cells were serum deprived for 24 h), 100 ⊙M BOLD-100, olaparib (1 ⊙M) or the combination at 72 h. Significantly increased autophagic vacuoles were seen in cells treated with both BOLD-100 and olaparib. ANOVA, $p < 0.001$; *p <0.001 for treatment versus vehcile. (D) Annexin V-FITC assay was used to measure apoptosis levels in MDA-MB-231 cells: vehicle alone, positive control (10 nM doxorubicin), 100 ⊙M BOLD-100, olaparib (1 ⊙M) or the combination at 72 h. ANOVA, $p < 0.002$; *p <0.03 for treatment versus vehcile.

Table 2: MDA-MB-231 *in vivo* xenograft study design as of Day 1

Group	n	Treatment Regimen for BOLD-100				Treatment Regimen for olaparib			
		Drug	Route	mg/kg	Schedule	Drug	Route	mg/kg	Schedule
#1	8	Vehicle	iv	--	qd4 to end	--	--	--	--
#2	8	BOLD-100	iv	30	qd4 to end	--	--	--	--
#3	8	BOLD-100	iv	50	qwk to end	--	--	--	--
#4	8	olaparib	po	50	qd x 32 (start on Day 2)	--	--	--	--
#5	8	BOLD-100	iv	30	q4d to end	olaparib	50	po	qd x 32 (start on Day 2)
#6	8	BOLD-100	iv	50	qwk to end	olaparib	50	po	qd x 32 (start on Day 2)

2.5. Combination of BOLD-100 and Olaparib suppressed growth of TNBC tumors

To further validate the efficacy of BOLD-100 and olaparib in vivo, we tested this combination in MDA-MB-231 breast cancer xenografts (Figure 7). Female nude mice with established subcutaneous MDA-MB-231 tumors were treated in accordance with the protocol summarized in Table 2 in six groups. Distribution of tumor volume in each group on Day 24 is shown in box and whisker plots (Figure 7A). Group 1 received saline, and served as the control group for analysis of tumor growth inhibition (TGI) and as a standard of statistical comparison for all treatment groups. Two different BOLD-100 regimens were followed: Group 2 mice received BOLD-100 at 30 mg/kg while Group 3 animals received BOLD-100 at 50 mg/kg. Group 4 animals received olaparib at 50 mg/kg. Group 5 animals received BOLD-100 at 30 mg/kg in combination with olaparib. Group 6 animals received BOLD-100 at 50 mg/kg in combination with olaparib. Mean tumor volume (MTV) in Group 3 that received 50 mg/kg BOLD-100 as a monotherapy showed 45% tumor growth inhibition (TGI) that differed significantly ($p<0.05$) from the control Group 1. Tumors treated with the combination of 50 mg/kg BOLD-100 and olaparib (Group 6) showed a 63% TGI that differed significantly ($p<0.05$) from the control Group 1 and olaparib monotherapy (Group 4) but was not significantly different from BOLD-100 50 mg/kg monotherapy (Group 3). Furthermore, median tumor growth was delayed for combination of 50 mg/kg BOLD-100 and olaparib (Group 6) compared to the control and all other treatment groups (Figure 7B). Percent group mean body weight did not show any significant changes from Day 1 through Day 24 (Supplement Figure S2). Assessment of ⊙H2AX protein by immunohistochemistry showed increased levels in MDA-MB-231 tumors treated with BOLD-100 (50 mg/kg; Group 3) and combination of 50 mg/kg BOLD-100 and olaparib (Group 6) compared with vehicle (Group 1) or olaparib treated (Group 4) (Figure 8). Collectively, these results showed that BOLD-100 is effective in decreasing TNBC tumor growth in vivo.

Peer-reviewed version available at Cancers 2020, 12, 2647; doi:10.3390/cancers12092647

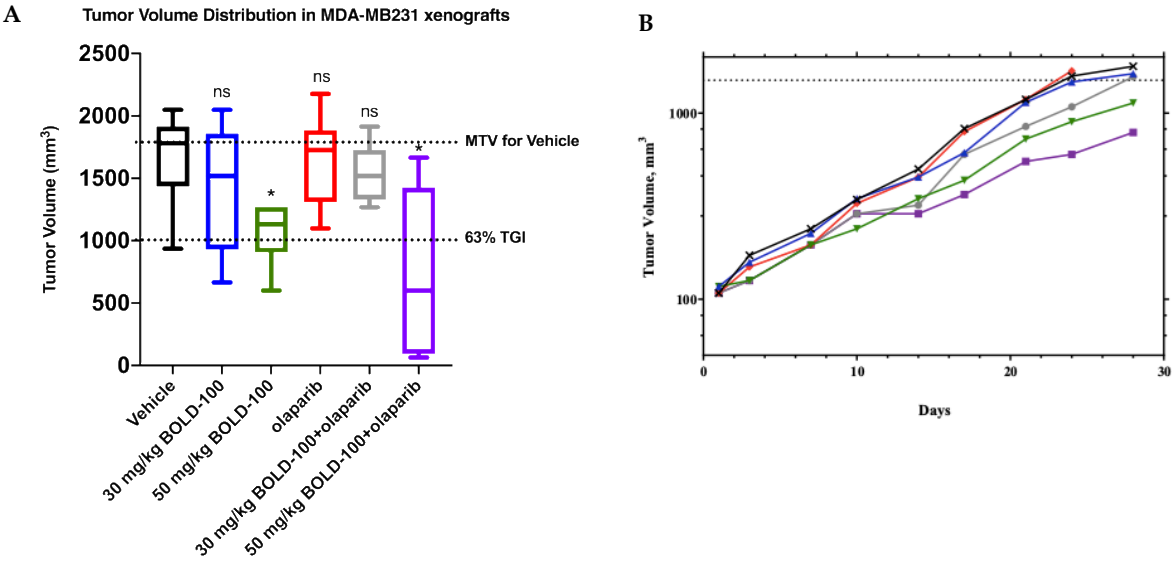

Figure 7. Combination of BOLD-100 and olaparib suppressed growth of TNBC xenografts. (A) Box and whisker plot showing distribution of tumor volume in each group of nude mice with MDA-MB-231 xenografts on Day 24 after treatment. Vehicle group received saline, and served as the control group for analysis and comparisons of the median tumor volumes (MTVs) and tumor growth inhibition (TGI; defined as the difference between MTV of treated and control mice on Day 24). MTV of tumors that received 50 mg/kg BOLD-100 as a monotherapy showed 45% tumor growth inhibition (TGI) that differed significantly ($p<0.05$) from vehicle. Tumors treated with the combination of 50 mg/kg BOLD-100 and olaparib showed a 63% TGI, (TGI>60% suggest a potential therapeutic activity), that differed significantly (*$p\leq0.05$, Mann-Whitney test) from vehicle or olaparib monotherapy but was not significantly different from BOLD-100 50 mg/kg. ns, not significant. (B) The median tumor volumes in each treatment group were plotted as a function of time. For both graphs, colors are: vehicle (black), 30 mg/kg BOLD-100 (blue), 50 mg/kg BOLD-100 (green), olaparib (red), 30 mg/kg BOLD-100+olaparib (grey) and 50 mg/kg BOLD-100+olaparib (purple).

Peer-reviewed version available at Cancers 2020, 12, 2647; doi:10.3390/cancers12092647

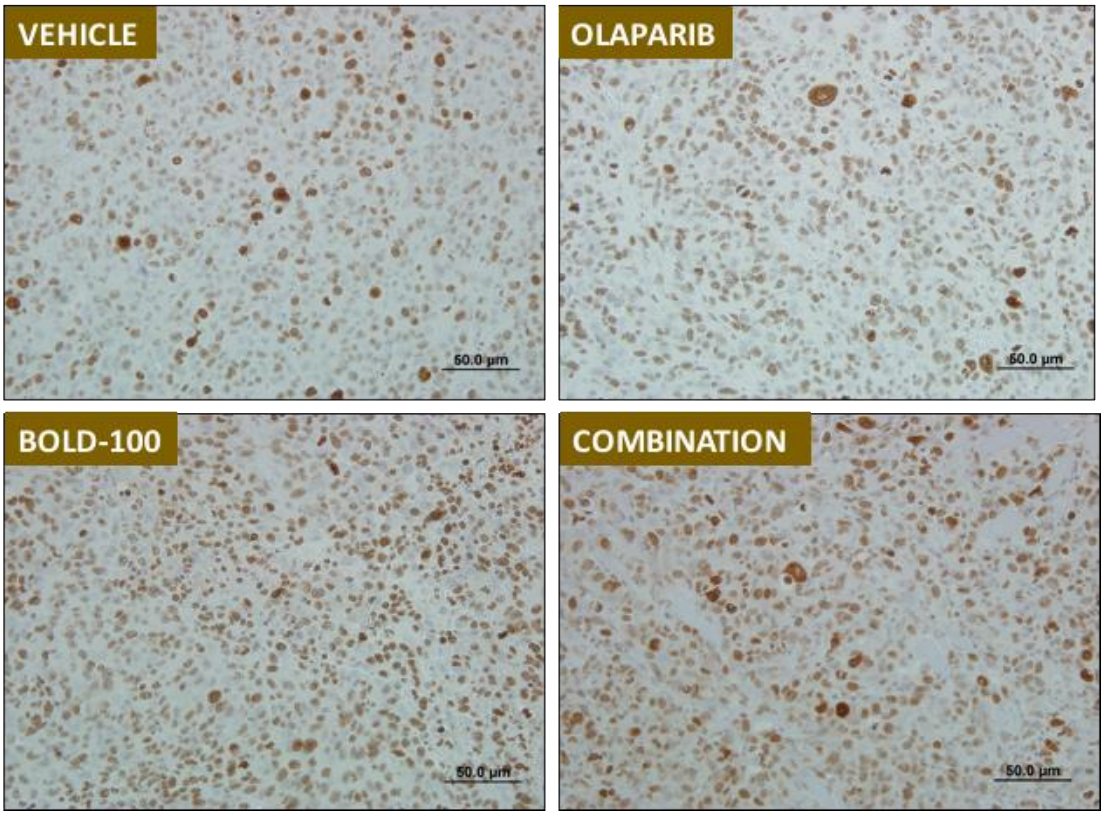

Figure 7. Treatment with BOLD-100 or BOLD-100+olaparib increased γH2AX protein levels in MDA-MB-231 xenografts. Immunohistochemical (IHC) γH2AX staining show increased protein levels (brown) in tumors treated with BOLD-100 or BOLD-100+olaparib compared with vehicle or olaparib only treated tumors.

3. Discussion

BOLD-100 is a novel small molecule that showed modest anti-tumor activity in a Phase I clinical trial [12]. Mechanistically, BOLD-100 has been shown to down-regulate GRP78 in stressed cancer cells [13] and trigger immunogenic cell death through the PERK/EIF2a branch of the UPR accompanied by ROS production, release of high mobility group box 1 (HMGB1) and ATP secretion via autophagy [32]. A comprehensive study with 23 cell lies that response to BOLD-100 can vary and in certain cells cell cycle (via G2 cell cycle arrest), DNA repair, and metabolism are affected [15]. Here we show that under unstressed conditions, in both ER+ and ER- breast cancer cells, BOLD-100 inhibits cell proliferation. BOLD-100 treatment in ER+ breast cancer cells, significantly altered genes in pathways involved in DNA repair, cell cycle and nucleotide biosynthesis (Figure 3A & Supplement Table S1). Mechanistically, BOLD-100 induces G2/M cells cycle arrest, ROS and ⊚H2AX, and potentially halts autophagy and promotes cell death via apoptosis.

Our gene-metabolite integration model in MCF7 cells offers novel molecular changes associated with BOLD-100 in breast cancer. Downregulation of genes such as ATM or BRCA1 suggest that BOLD-100 treatment leads to the disruption of pathways associated with the DNA repair pathway. Furthermore, levels of ⊚H2AX, a marker of DSB [33], were increased in BOLD-100 treated breast cancer cells (Figure 3C and Figure 6A) and tumors (Figure 8). Monitoring of DSB in human tissues such as blood or skin provides a minimally invasive strategy to monitor efficacy of therapeutics in patients [29], and therefore, could also be a useful biomarker to evaluate the efficacy of BOLD-100. Furthermore, recent studies have reported changes in cellular metabolite profile [34] or protein associated with specific metabolic pathways [35] including DDR following treatment with BOLD-100. Consistently, our data shows in breast cancer cells showed an increase in DNA damage, as shown by increase in ⊚H2AX. Specifically, citrate was significantly increased (11-fold) in BOLD-100 treated MCF7 cells (Figure 3D). While further research is needed to define the cellular metabolic changes associated with BOLD-100 treatment in cancer, it is worthwhile to note that citrate is a key

Peer-reviewed version available at Cancers 2020, 12, 2647; doi:10.3390/cancers12092647

metabolite in the tricarboxylic acid cycle (TCA) and increased citrate levels in the cytosol can inhibit growth of cancer cells by G2/M arrest [36].

Upregulated genes (Figure 3A) and protein (Figure 3C) that were increased with BOLD-100 treatment included CYP1B1, which suggested a role of this enzyme in metabolizing the drug within cells. CYP1B1 is a dioxin inducible oxidoreductase and a member of the cytochrome P450 superfamily [37,38]. Single-nucleotide polymorphisms (SNPs) associated with CYP1B1 have been reported to a possible biomarker for therapy response in cancer [24,39,40]. Further studies into the role of CYP1B1 in BOLD-100 mediated inhibition of cancer cell proliferation will be needed to understand whether SNPs associated with this gene can affect drug sensitivity in different cancers.

In TNBC, where there is a lack of targeted therapy options, our data suggests that BOLD-100 alone or in combination with olarapib is effective in inhibiting tumor growth (Figure 7). Olaparib is the only FDA-approved therapy for germline BRCA mutated advanced ovarian cancer and metastatic breast cancer. Olaparib inhibits BRCA1/2 mutated cancer cells that have an increased reliance on PARP to repair their damaged DNA and therefore are more vulnerable to olaparib treatment [8]. Significantly downregulated genes and proteins in MCF7(2) prompted us to test of efficacy of BOLD-100 in combination anticancer therapies that target the DNA in TNBC. Although GRP78 protein levels did not change in MCF7(2) or MDA-MB-231 cells (Supplement Figure S1 A and B) following BOLD-100 treatment combination of BOLD-100 and olaparib significantly reduced MDA-MB-231 tumor volume and induced increase in ⊚H2AX compared to control. Currently, BOLD-100 is being tested in combination with other anti-cancer agents for the treatment of various gastrointestinal cancers, including gastric, pancreatic, colorectal and bile duct cancers (NCT04421820). Our study provides a comprehensive view of genes, proteins and metabolites that are changed associated with inhibition of cell growth with BOLD-100 in breast cancer cells. Particularly in TNBC with defective DNA repair pathways, there is potential to use BOLD-100 in effective combination therapeutic approaches.

4. Materials and Methods

4.1. Cell culture and reagents

ER+ MCF7 (originally obtained from the Barbara A. Karmanos Cancer Institute, Detroit, MI), MCF7(2) (a MCF7 derivative cell line that shows increased sensitivity to estrogen; [16] and TNBC cell lines, MDA-MB-231 and MDA-MB-468 (originally obtained from American Type Culture Collection, Manassas, VA), were provided by the Tissue Culture Shared Resources at Georgetown University Medical Center. ER+ breast cancer cells line, MDA-MB-175, was purchased from American Type Culture Collection (ATCC; Manassas, VA). All cell lines were grown in IMEM (Life Technologies, Grand Island, NY; A10489-01) media supplemented with 5% fetal bovine serum. BOLD-100 (formerly IT-139, NKP1339 and KP1339) was provided by Intezyne Biosciences, Inc. (Tampa, FL). For in vitro assays, dimethyl sulfoxide (DMSO) was used at the diluent and negative control (0.2%). Olaparib (AZD-2281) was purchased from Selleck (Houston, TX). All cells were authenticated by DNA fingerprinting and tested regularly for Mycoplasma infection. All other chemicals were purchased from Sigma-Aldrich.

4.2. Cell proliferation and viability

To determine cell growth, cells were plated in 96-well plates at the following densities: MCF7 and MCF7(2) cells at 4-5×103 cells/well. At 24 h, cells were treated with specified drugs for 72 h (or otherwise indicated). For all t=0 plates, cell media was removed and processed for cell proliferation within 24 h when treatment began. The purpose of the t=0 plate was to provide a baseline level of cell growth at the beginning of treatment to compare growth with treatment at specified time-points. After treatment, media were removed, and plates were stained with a solution containing 0.5% crystal violet and 25% methanol, rinsed, dried overnight, and re-suspended in citrate buffer (0.1 M sodium citrate in 50% ethanol). Intensity of staining, assessed at 570 nm and quantified using a VMax

Peer-reviewed version available at Cancers 2020, 12, 2647; doi:10.3390/cancers12092647

kinetic microplate reader (Molecular Devices Corp., Menlo Park, CA), is directly proportional to cell number [17,18].

4.3. Cell cycle analysis

Cells were grown at 70% confluence on 100 mm in complete growth medium for 24 h. The following day, cells were treated with vehicle or 100 ◎M BOLD-100 for an additional 72 h. Cells were then fixed in ethanol, and analyzed by the Flow Cytometry Shared Resource according to the method of Vindelov et al [19]. Each experiment was repeated at least three times.

4.4. Analysis of cellular ROS Assay

ROS production was measured by using 2′,7′-dichlorodihydrofluorescein diacetate (DCFDA) as an indicator (ab113851; Abcam, Cambridge, MA). Briefly, cells were plated at 70% confluence on 100 mm dishes in complete media. At 24 h, cells were collected by trypsinization and stained with 10 ◎M DCFDA dye for 40 min at 37oC. About 1x105 cells were aliquoted and treated with the following for 4 h: 100 ◎M tert-butyl hydrogen peroxide (TBHP; positive control), DMSO alone (negative control), and indicated concentrations of BOLD-100. Fluorescence signal was read at Ex/Em: 485/535 nm through the Flow Cytometry Shared Resource. Changes in ROS levels were determined as a percentage of control after background subtraction.

4.5. Western blotting

Total protein (~20 ◎g) was isolated from cells following 72 h treatment or vehicle control (0.02% DMSO or ethanol) for protein analysis as previously describe [17,18]. Tris-glycine gels were used for all analysis except for BRCA1, ATM and the respective loading control where Tris-acetate gels were used to accommodate higher molecular weights of these proteins. The following antibodies were used: Actin (#4967), ATM (#2873), BRCA1 (#9010), ◎H2AX (#80312), Rad51 (#8875), total-H2AX (#7631), p62 (#2947) and LC3BII (#2775) were from Cell Signaling (Danvers, MA); CYP1B1 (ab185954) was from Abcam; ◎-tubulin (T7816) was from Sigma; DNA/RNA damage antibody (SMC-155) was from StressMarq (Victoria, CAN) and actin (#47778) was from Santa Cruz Biotechnology (Santa Cruz, CA).

4.6. Generation, analysis and integration of transcriptomics and metabolomics data from MCF7(2) cells

Transcriptome data - We obtained and analyzed gene expression and untargeted metabolomics data from MCF7(2) cells treated with vehicle alone or 100 ◎M BOLD-100. Microarray analysis was performed using three biological replicates using Affymetrix HG U133 Plus 2.0 microarray at our Genomics and Epigenomics Shared Resources. Briefly, total RNA was extracted using the RNeasy kit (Qiagen, Valencia, CA, USA). RNA labeling and hybridization were performed according to the Affymetrix protocol for one-cycle target labeling. For each experiment, fragmented cDNA was hybridized in triplicates to Affymetrix GeneChip HG-U95 arrays (Affymetrix, Santa Clara, CA). Affymetrix data analysis included pre-processing of the probe-level Affymetrix data (CEL files). Affymetrix data analysis included pre-processing of the probe-level Affymetrix data (CEL files).

Metabolomics data - Metabolomics analysis was done through the Metabolomics Shared Resource Core (MSRC) at Georgetown University Medical Center with four biological replicates from each of the two groups, and two technical replicates per sample. LC-MS was used to analyze the MSRC samples. Briefly, metabolite extraction was performed as described by Sheikh et al. [51]. Briefly, the residual pellet was resuspended in 200 µL of solvent A (98% water, 2% ACN and 0.1% formic acid) for Ultra-performance liquid chromatography-electro-spray ionization quadrupole-time-of-flight mass spectrometry (UPLC-ESI-Q-TOFMS) analysis. Mass spectrometry was performed on a Q-TOF Premier (Waters) operating in either negative-ion (ESI-) or positive-ion (ESI+) electro-spray ionization mode with a capillary voltage of 3200 V and a sampling cone voltage of 20 V in negative mode and 35 V in positive mode. The cone gas flow was 25 L/h, and the source temperature was 120°C. Accurate mass was maintained by introduction of LockSpray interface of

Peer-reviewed version available at Cancers 2020, 12, 2647; doi:10.3390/cancers12092647

sulfadimethoxine (311.0814 [M+H]+ or 309.0658 [M-H]−). Data were acquired in centroid mode from 50 to 850 m/z in MS scanning. Centroided and integrated mass spectrometry data from the UPLC-TOFMS was processed to generate a multivariate data matrix using MarkerLynx (Waters).
(Accession numbers for all molecular data generated will be available during the review of this manuscript.) Network analysis of the top 2000 differentially expressed (DE) genes, ranked by P-value, [IPA Core Analysis (QIAGEN Inc., https://www.qiagenbioinformatics.com/products/ingenuity-pathway-analysis)] identified disease and functional pathways enriched in differentially expressed genes (Table 1). Each of the mutually exclusive networks of DE genes were input into STITCH [20] along with all DE metabolites to integrate the gene and protein expression datasets and expand the networks to include common interacting neighbors from the STITCH database. The resulting networks for each DE set were integrated and pruned of both nodes not detected as differentially expressed in the dataset including subnetworks isolated from the largest interconnected sets. The networks were visualized using Cytoscape [21], with genes represented as rectangles and metabolites as triangles, with the log2 fold change overlaid scaled from low (green) to high (red) expression.

4.7. Quantification of citrate/isocitrate

Total cellular citrate/isocitrate levels were detected by UPLC-MS in three replicates of MCF7(2) and MDA-MB-231 cells treated with vehicle alone (DMSO) or 100 ◎M BOLD-100. Briefly, samples were resolved on an Acquity BEH C18 1.7μm, 2.1 x 100 mm column online with a triple quadrupole mass spectrometer (Xevo-TQ-S, Waters Corporation, USA) operating in the multiple reaction monitoring (MRM) mode. The sample cone voltage and collision energies were optimized for the analyte to obtain maximum ion intensity for parent and daughter ions using "IntelliStart" feature of MassLynx software (Waters Corporation, USA). Signal intensities from all MRM Q1/Q3 ion pairs for the analyte were ranked to ensure selection of the most intense precursor and fragment ion pair for MRM-based quantitation. The metabolite ratios were calculated by normalizing the peak area of endogenous metabolites within cell samples normalized to the internal standard (IS-citric acid-d4) and respective levels of proteins from each cell sample. Analysis was performed with a calibration curve, the sample queue was randomized and solvent blanks were injected to assess sample carryover. MRM data were processed using Target Lynx 4.1. The relative quantification values of analytes were determined by calculating the ratio of peak areas of transitions of samples normalized to the peak area of the internal standard.

4.8. TNBC xenografts and in vivo studies

In vivo assessment of the efficacy of BOLD-100 and olaparib, alone or in combination, against MDA-MB-231 TNBC xenografts in nice weeks old female NCr nude mice (Crl:NU(NCr)-Foxn1nu, Charles River) through a contract between Intezyne Technologies and Charles River Discovery Services North Carolina. Briefly, cells were implanted subcutaneously and tumors were allowed to form to a mean volume of 107 mm3. Bold-100 dosing solution of 5 mg/mL in saline was freshly prepared just prior to administration. Once solubilized in saline, the 5 mg/mL solution was further diluted to 3 mg/mL. The 5 and 3 mg/mL solutions provided the 50 and 30 mg/kg dosages in a dosing volume of 10 mL/kg (200 μL per 20 g animal), scaled to the weight of each animal. Olaparib was freshly prepared weekly by dissolving in one volume of DMSO and further diluting in nine volumes of 20% (2-Hydroxypropyl)-β-cyclodextrin (HPBCD) to achieve a 5 mg/mL dosing solution in 10% DMSO in 20% HPBCD that was administered at 10 mL/kg (50 mg/kg) scaled to the weight of each animal. All dosing solutions were protected from light until dosed. On day 1, mice were divided into six groups (n=8) and treated as summarized in Table 2. Vehicle control (saline) and BOLD-100 was administered intravenously (i.v.) and olaparib was administered daily orally (p.o.) starting at Day 2 until end of study at Day 28. Tumors were measured twice a week and the study was terminated on Day 28. Tumors were processed for histology. Outcome was determined based on tumor growth inhibition (TGI), which was defined as the difference between the median tumor volumes (MTV) of treated and control mice on day 24, the last day all mice in control Group 1 remained on the study (%TGI = [1–(MTVdrug-treated/MTVcontrol)] x 100). The results were analyzed utilizing the Mann-

Peer-reviewed version available at Cancers 2020, 12, 2647; doi:10.3390/cancers12092647

Whitney U-test, and were deemed statistically significant at $p \leq 0.05$. Any treatment that produced at least 60% TGI was considered potentially therapeutically active. Drug tolerability was assessed by body weight measurements (Supplement Figure S2) and by frequent observation.

4.9. Immunohistochemistry (IHC)

Immunostaining was performed on 5 μm thick sections from MDA-MB-231 xenografts embedded in paraffin with an antibody to ◎H2AX [phospho S139] (abcam #ab81299) at 1:4000 or a non-specific negative control antibody using the diaminobenzidine (DAB) method at the Histopathology and Tissue Shared Resource. Slides were photographed with bright field using an Olympus IX-71 Inverted microscope at the Microscopy Shared Resource.

4.10. Reverse phase protein array (RPPA)

Whole cell lysates from sub-confluent MCF7(2) cells treated with either 100 mM BOLD-100 or vehicle alone (n=3 for each condition) for 72 h were analyzed for 305 proteins and phosphoproteins at the RPPA core at the University of Texas MD Anderson Cancer Center [22] following their sample preparation protocol. Briefly, cells were washed in ice-cold PBS, then lysed in RPPA lysis buffer [1% Triton X-100, 50mM HEPES, pH 7.4, 150mM NaCl, 1.5mM MgCl2, 1mM EGTA, 100mM NaF, 10mM Na pyrophosphate, 1mM Na3VO4, 10% glycerol, with freshly added protease [#05056489001] and phosphatase [#04906837001] (Roche, Germany) for 30 minutes on ice, centrifuged for 15 minutes at 14,000 rpm, and the supernatant collected. Protein concentration was determined using a Pierce 660-nm Protein Assay (ThermoFisher, Waltham, MA). Cell lysates were mixed with sample buffer, boiled and stored at –80oC until sample submission. Relative quantification of each sample was compared with a reference standard curve generated from control lysates. All data points were normalized for protein loading and transformed to linear value that were used in this study.

4.11. Statistical analysis for cell proliferation experiments

Statistical analyses were performed using the Prism 7 (La Jolla, CA). All experimental values were expressed as mean ± standard errors. Differences between two groups were determined by using the unpaired Student t-test, and p-values less than 0.05 were considered as statistically significant. Nature of interaction between drugs was defined by measuring the R-index (RI). The RI values were obtained by calculating the expected cell survival (Sexp; the product of survival obtained with drug A alone and the survival obtained with drug B alone) and dividing Sexp by the observed cell survival in the presence of both drugs (Sobs). Sexp/Sobs > 1.0 indicates a synergistic interaction [23].

5. Conclusions

BOLD-100 is a novel anticancer drug that has shown manageable safety profile in a clinical trial. While BOLD-100 is known to decrease the levels of GRP78 in stressed breast cancer cells, the mechanism of action in non-stressed remain unknown. Using an unbiased approach, we evaluated the molecular changes associated with BOLD-100 mediated inhibition of cell growth in breast cancer cells and found DNA repair pathways to be significantly impaired. Therefore, the combination of BOLD-100 with standard anticancer agents that target the DNA, particularly in TNBC, is a reasonable combination strategy. Together, our study contributes to the growing body of work focused on BOLD-100, which shows that effect of this drug as an anticancer therapy is cell context dependent. Further studies are warranted to assess whether BOLD-100 could be an effective therapy for metastatic breast cancer.

Supplementary Materials: Provided in Appendix A

Author Contributions: Conceptualization, S.B., A.N.S.-H., methodology, A.N.S-H., M.M., L.J.; Performing experiments and analysis, I.C., Y.F.; Data interpretation, S.B., I.C., Y.F., M.M., L.J., A.N.S.-H.; Writing (original draft), S.B., I.C., A.N.S.-H.; Project administration, A.N.S.-H. All authors have read and agree to the published version of the manuscript.

Peer-reviewed version available at *Cancers* **2020**, *12*, 2647; doi:10.3390/cancers12092647

Funding: This work was partly supported by Public Health Service NIH grant R01CA201092 to ANS-H. Technical services were provided by the following shared resources at Georgetown University Medical Center: Genomics and Epigenomics, Flow Cytometry and Tissue Culture Core Shared Resources that were funded through NIH grant 1P30-CA-51008 (Lombardi Comprehensive Cancer Center Support Grant). RPPA data was generated with support from NIH grant CA16672 (MD Anderson Cancer Center).

Acknowledgments: We thank Diane M. Demas for excellent technical support with the *in vitro* assays. We also thank the Georgetown Breast Cancer Advocates (GBCA) for the patient perspective they provided for this study.

Conflicts of Interest: SB was formerly employed by Intezyne Technologies, Inc, and is currently a Consultant for Bold Therapeutics, Inc. SB contributed to concept design, revision and final approval of present article. AS-H has received a research grant from Intezyne Technologies, Inc to partly support this project. The remaining authors declare that the research was conducted in the absence of any commercial or financial relationships that could be construed as a potential conflict of interest.

References

1. Clarke, R.; Skaar, T.; Baumann, K.; Leonessa, F.; James, M.; Lippman, J.; Thompson, E.W.; Freter, C.; Brunner, N. Hormonal carcinogenesis in breast cancer: cellular and molecular studies of malignant progression. Breast Cancer Res Treat 1994, 31, 237-248.
2. Clarke, R.; Shajahan, A.N.; Riggins, R.B.; Cho, Y.; Crawford, A.; Xuan, J.; Wang, Y.; Zwart, A.; Nehra, R.; Liu, M.C. Gene network signaling in hormone responsiveness modifies apoptosis and autophagy in breast cancer cells. J Steroid Biochem Mol Biol 2009, 114, 8-20.
3. Iorfida, M.; Mazza, M.; Munzone, E. Fulvestrant in Combination with CDK4/6 Inhibitors for HER2- Metastatic Breast Cancers: Current Perspectives. Breast Cancer (Dove Med Press) 2020, 12, 45-56, doi:10.2147/BCTT.S196240.
4. Lynce, F.; Shajahan-Haq, A.N.; Swain, S.M. CDK4/6 inhibitors in breast cancer therapy: Current practice and future opportunities. Pharmacol Ther 2018, 191, 65-73, doi:10.1016/j.pharmthera.2018.06.008.
5. Spring, L.M.; Wander, S.A.; Andre, F.; Moy, B.; Turner, N.C.; Bardia, A. Cyclin-dependent kinase 4 and 6 inhibitors for hormone receptor-positive breast cancer: past, present, and future. Lancet 2020, 395, 817-827, doi:10.1016/S0140-6736(20)30165-3.
6. Waks, A.G.; Winer, E.P. Breast Cancer Treatment: A Review. JAMA 2019, 321, 288-300, doi:10.1001/jama.2018.19323.
7. Hurvitz, S.; Mead, M. Triple-negative breast cancer: advancements in characterization and treatment approach. Curr Opin Obstet Gynecol 2016, 28, 59-69, doi:10.1097/GCO.0000000000000239.
8. Griguolo, G.; Dieci, M.V.; Miglietta, F.; Guarneri, V.; Conte, P. Olaparib for advanced breast cancer. Future Oncol 2020, doi:10.2217/fon-2019-0689.
9. Augusto, T.V.; Correia-da-Silva, G.; Rodrigues, C.M.P.; Teixeira, N.; Amaral, C. Acquired resistance to aromatase inhibitors: where we stand! Endocr Relat Cancer 2018, 25, R283-R301, doi:10.1530/ERC-17-0425.
10. Droog, M.; Beelen, K.; Linn, S.; Zwart, W. Tamoxifen resistance: from bench to bedside. Eur J Pharmacol 2013, 717, 47-57, doi:10.1016/j.ejphar.2012.11.071.
11. Zhao, Y.; Butler, E.B.; Tan, M. Targeting cellular metabolism to improve cancer therapeutics. Cell Death Dis 2013, 4, e532, doi:10.1038/cddis.2013.60.
12. Burris, H.A.; Bakewell, S.; Bendell, J.C.; Infante, J.; Jones, S.F.; Spigel, D.R.; Weiss, G.J.; Ramanathan, R.K.; Ogden, A.; Von Hoff, D. Safety and activity of IT-139, a ruthenium-based compound, in patients with advanced solid tumours: a first-in-human, open-label, dose-escalation phase I study with expansion cohort. ESMO Open 2016, 1, e000154, doi:10.1136/esmoopen-2016-000154.
13. Bakewell, S.J.; Rangel, D.F.; Ha, D.P.; Sethuraman, J.; Crouse, R.; Hadley, E.; Costich, T.L.; Zhou, X.; Nichols, P.; Lee, A.S. Suppression of stress induction of the 78-kilodalton glucose regulated protein (GRP78) in cancer by IT-139, an anti-tumor ruthenium small molecule inhibitor. Oncotarget 2018, 9, 29698-29714, doi:10.18632/oncotarget.25679.

Peer-reviewed version available at Cancers 2020, 12, 2647; doi:10.3390/cancers12092647

14. Gifford, J.B.; Huang, W.; Zeleniak, A.E.; Hindoyan, A.; Wu, H.; Donahue, T.R.; Hill, R. Expression of GRP78, Master Regulator of the Unfolded Protein Response, Increases Chemoresistance in Pancreatic Ductal Adenocarcinoma. Mol Cancer Ther 2016, 15, 1043-1052, doi:10.1158/1535-7163.MCT-15-0774.
15. Schoenhacker-Alte, B.; Mohr, T.; Pirker, C.; Kryeziu, K.; Kuhn, P.S.; Buck, A.; Hofmann, T.; Gerner, C.; Hermann, G.; Koellensperger, G., et al. Sensitivity towards the GRP78 inhibitor KP1339/IT-139 is characterized by apoptosis induction via caspase 8 upon disruption of ER homeostasis. Cancer Lett 2017, 404, 79-88, doi:10.1016/j.canlet.2017.07.009.
16. James, M.R.; Skaar, T.C.; Lee, R.Y.; MacPherson, A.; Zwiebel, J.A.; Ahluwalia, B.S.; Ampy, F.; Clarke, R. Constitutive expression of the steroid sulfatase gene supports the growth of MCF-7 human breast cancer cells in vitro and in vivo. Endocrinology 2001, 142, 1497-1505, doi:10.1210/endo.142.4.8091.
17. Shajahan-Haq, A.N.; Cook, K.L.; Schwartz-Roberts, J.L.; Eltayeb, A.E.; Demas, D.M.; Warri, A.M.; Facey, C.O.; Hilakivi-Clarke, L.A.; Clarke, R. MYC regulates the unfolded protein response and glucose and glutamine uptake in endocrine resistant breast cancer. Mol Cancer 2014, 13, 239, doi:10.1186/1476-4598-13-239.
18. Shajahan-Haq, A.N.; Boca, S.M.; Jin, L.; Bhuvaneshwar, K.; Gusev, Y.; Cheema, A.K.; Demas, D.D.; Raghavan, K.S.; Michalek, R.; Madhavan, S., et al. EGR1 regulates cellular metabolism and survival in endocrine resistant breast cancer. Oncotarget 2017, 8, 96865-96884, doi:10.18632/oncotarget.18292.
19. Vindeløv, L.L.; Christensen, I.J.; Nissen, N.I. A detergent-trypsin method for the preparation of nuclei for flow cytometric DNA analysis. Cytometry 1983, 3, 323-327, doi:10.1002/cyto.990030503.
20. Szklarczyk, D.; Franceschini, A.; Wyder, S.; Forslund, K.; Heller, D.; Huerta-Cepas, J.; Simonovic, M.; Roth, A.; Santos, A.; Tsafou, K.P., et al. STRING v10: protein-protein interaction networks, integrated over the tree of life. Nucleic Acids Res 2015, 43, D447-452, doi:10.1093/nar/gku1003.
21. Lopes, C.T.; Franz, M.; Kazi, F.; Donaldson, S.L.; Morris, Q.; Bader, G.D. Cytoscape Web: an interactive web-based network browser. Bioinformatics 2010, 26, 2347-2348, doi:10.1093/bioinformatics/btq430.
22. Hennessy, B.T.; Lu, Y.; Gonzalez-Angulo, A.M.; Carey, M.S.; Myhre, S.; Ju, Z.; Davies, M.A.; Liu, W.; Coombes, K.; Meric-Bernstam, F., et al. A Technical Assessment of the Utility of Reverse Phase Protein Arrays for the Study of the Functional Proteome in Non-microdissected Human Breast Cancers. Clin Proteomics 2010, 6, 129-151, doi:10.1007/s12014-010-9055-y.
23. Romanelli, S.; Perego, P.; Pratesi, G.; Carenini, N.; Tortoreto, M.; Zunino, F. In vitro and in vivo interaction between cisplatin and topotecan in ovarian carcinoma systems. Cancer Chemother Pharmacol 1998, 41, 385-390, doi:10.1007/s002800050755.
24. Abdul Aziz, A.A.; Md Salleh, M.S.; Mohamad, I.; Krishna Bhavaraju, V.M.; Mazuwin Yahya, M.; Zakaria, A.D.; Hua Gan, S.; Ankathil, R. Single-nucleotide polymorphisms and mRNA expression of. J Genet 2018, 97, 1185-1194.
25. Klinakis, A.; Karagiannis, D.; Rampias, T. Targeting DNA repair in cancer: current state and novel approaches. Cell Mol Life Sci 2020, 77, 677-703, doi:10.1007/s00018-019-03299-8.
26. Zhao, W.; Feng, H.; Sun, W.; Liu, K.; Lu, J.J.; Chen, X. Tert-butyl hydroperoxide (t-BHP) induced apoptosis and necroptosis in endothelial cells: Roles of NOX4 and mitochondrion. Redox Biol 2017, 11, 524-534, doi:10.1016/j.redox.2016.12.036.
27. Jhan, J.R.; Andrechek, E.R. Triple-negative breast cancer and the potential for targeted therapy. Pharmacogenomics 2017, 18, 1595-1609, doi:10.2217/pgs-2017-0117.
28. Srinivas, U.S.; Tan, B.W.Q.; Vellayappan, B.A.; Jeyasekharan, A.D. ROS and the DNA damage response in cancer. Redox Biol 2019, 25, 101084, doi:10.1016/j.redox.2018.101084.
29. Bonner, W.M.; Redon, C.E.; Dickey, J.S.; Nakamura, A.J.; Sedelnikova, O.A.; Solier, S.; Pommier, Y. GammaH2AX and cancer. Nat Rev Cancer 2008, 8, 957-967, doi:10.1038/nrc2523.
30. Rogakou, E.P.; Pilch, D.R.; Orr, A.H.; Ivanova, V.S.; Bonner, W.M. DNA double-stranded breaks induce histone H2AX phosphorylation on serine 139. J Biol Chem 1998, 273, 5858-5868, doi:10.1074/jbc.273.10.5858.

Peer-reviewed version available at Cancers 2020, 12, 2647; doi:10.3390/cancers12092647

31. Klionsky, D.J.; Abdelmohsen, K.; Abe, A.; Abedin, M.J.; Abeliovich, H.; Acevedo Arozena, A.; Adachi, H.; Adams, C.M.; Adams, P.D.; Adeli, K., et al. Guidelines for the use and interpretation of assays for monitoring autophagy (3rd edition). Autophagy 2016, 12, 1-222, doi:10.1080/15548627.2015.1100356.
32. Wernitznig, D.; Kiakos, K.; Del Favero, G.; Harrer, N.; Machat, H.; Osswald, A.; Jakupec, M.A.; Wernitznig, A.; Sommergruber, W.; Keppler, B.K. First-in-class ruthenium anticancer drug (KP1339/IT-139) induces an immunogenic cell death signature in colorectal spheroids in vitro. Metallomics 2019, 11, 1044-1048, doi:10.1039/c9mt00051h.
33. Kuo, L.J.; Yang, L.X. Gamma-H2AX - a novel biomarker for DNA double-strand breaks. In Vivo 2008, 22, 305-309.
34. Rusz, M.; Rampler, E.; Keppler, B.K.; Jakupec, M.A.; Koellensperger, G. Single Spheroid Metabolomics: Optimizing Sample Preparation of Three-Dimensional Multicellular Tumor Spheroids. Metabolites 2019, 9, doi:10.3390/metabo9120304.
35. Stultz, L.K.; Hunsucker, A.; Middleton, S.; Grovenstein, E.; O'Leary, J.; Blatt, E.; Miller, M.; Mobley, J.; Hanson, P.K. Proteomic analysis of the S. cerevisiae response to the anticancer ruthenium complex KP1019. Metallomics 2020, 12, 876-890, doi:10.1039/d0mt00008f.
36. Hung, K.C.; Wang, S.G.; Lin, M.L.; Chen, S.S. Citrate-Induced p85α-PTEN Complex Formation Causes G. Int J Mol Sci 2019, 20, doi:10.3390/ijms20092105.
37. Dutour, R.; Poirier, D. Inhibitors of cytochrome P450 (CYP) 1B1. Eur J Med Chem 2017, 135, 296-306, doi:10.1016/j.ejmech.2017.04.042.
38. Go, R.E.; Hwang, K.A.; Choi, K.C. Cytochrome P450 1 family and cancers. J Steroid Biochem Mol Biol 2015, 147, 24-30, doi:10.1016/j.jsbmb.2014.11.003.
39. Hertz, D.L.; Kidwell, K.M.; Seewald, N.J.; Gersch, C.L.; Desta, Z.; Flockhart, D.A.; Storniolo, A.M.; Stearns, V.; Skaar, T.C.; Hayes, D.F., et al. Polymorphisms in drug-metabolizing enzymes and steady-state exemestane concentration in postmenopausal patients with breast cancer. Pharmacogenomics J 2017, 17, 521-527, doi:10.1038/tpj.2016.60.
40. Vasile, E.; Tibaldi, C.; Leon, G.L.; D'Incecco, A.; Giovannetti, E. Cytochrome P450 1B1 (CYP1B1) polymorphisms are associated with clinical outcome of docetaxel in non-small cell lung cancer (NSCLC) patients. J Cancer Res Clin Oncol 2015, 141, 1189-1194, doi:10.1007/s00432-014-1880-3.